

# Observation of the Quantum Zeno Effect on a NISQ Device

Andrea Alessandrini,<sup>1</sup> Carola Ciaramelletti,<sup>2,1</sup> and Simone Paganelli<sup>1,\*</sup>

<sup>1</sup>*Dipartimento di Scienze Fisiche e Chimiche, Università dell'Aquila, via Vetoio, I-67100 Coppito-L'Aquila, Italy.*

<sup>2</sup>*Dipartimento di Ingegneria e Scienze dell'Informazione e Matematica, Università dell'Aquila, via Vetoio, I-67100 Coppito-L'Aquila, Italy.*

We study the Quantum Zeno Effect (QZE) on a single qubit on IBM Quantum Experience devices under the effect of multiple measurements. We consider two possible cases: the Rabi evolution and the free decay. In both cases we observe the occurrence of the QZE as an increasing of the survival probability with the number of measurements.

## I. INTRODUCTION

The QZE refers to the freezing of a system in a given state, or in a given subspace of the Hilbert space, due to frequent measurements applied during its evolution. The possibility that the lifetime of an unstable system could depend on the measuring process was first analyzed in [1] and then subsequently formalized in [2, 3], where the QZE name was given to this phenomenon. Since then, the QZE has attracted a lot of interest [4–11] and it has been observed experimentally in different contexts [12–17].

The QZE can be also due by the interaction with an external environment and produce a confinement into a subspace [18]. In this case, the coupling induces a dynamical superselection rule splitting the open system's Hilbert space into non-communicating quantum Zeno subspaces where coherent evolution can take place. Therefore, the QZE can be employed to control decoherence [8, 19–23].

Given an open system in an excited state, it starts to decay exponentially after a characteristic time  $T_E$ . For times shorter than  $T_E$ , quantum effects prevail, the evolution deviates from the exponential behavior [3, 9, 10, 24, 25] exhibiting a quadratic behavior: here QZE can occur. Nevertheless, the coupling with a continuous spectrum could give rise to extra contributions which must be added to the quadratic one that could possibly produce a speed up of the decay rate. This phenomenon is the so-called Quantum Anti-Zeno Effect (QAZE) [26–30]. Both the QZE and QAZE are characterized by two well defined times  $T_Z$  and  $T_{AZ}$ , respectively, where generically  $T_E > T_{AZ} > T_Z$ . If the time between measurements is much shorter than  $T_Z$ , then the QZE can be observed, while in the time region between  $T_Z$  and  $T_{AZ}$  the QAZE exists [28].

Concerning the possibility to observe the QZE on a Noisy Intermediate Scale Quantum (NISQ) device [37], simulations have been performed with ideal (noiseless and decoherence free) qubits [31, 32], and predictions have been formulated about the behavior of real ones [33, 34]. Furthermore, there are experiments involving

superconducting flux qubits [35] and about the observation of the QZE from measurement controlled qubit-bath interactions involving a transmon circuit [36].

In this paper, we show the observation of the QZE on real NISQ devices. In particular, we employed IBM Quantum Experience devices, which belong to the class of gate based quantum computers, consisting in superconducting Josephson junctions in transmon regime [38–40]. In Section II we describe the general problem of the QZE in two cases: the Rabi evolution and the free decay of a single qubit and how to ideally implement them on the online platform IBM Quantum Experience. In Section III, we give more insights about the implementations on real devices. Despite the big amount of noise, our results show a manifestation of the QZE in both the dynamics, with qualitative agreement with the theory.

## II. RABI EVOLUTION AND FREE EVOLUTION

In the present section, we describe two different time evolutions of a single qubit that we consider in this paper: the oscillations under a Rabi Hamiltonian and the free decay. The first case was already studied in [31] and [32], where the Quantum Zeno dynamics has been found by IBM Quantum Experience simulations. Here we briefly recall the model Hamiltonian and the measurement scheme, and in the next section we will compare the results of these simulations with the data obtained from a real IBM quantum computer. The Rabi Hamiltonian for a single qubit is

$$\hat{H} = \hbar\omega (|0\rangle\langle 1| + |1\rangle\langle 0|) = \hbar\omega\hat{\sigma}_x, \quad (1)$$

corresponding to the time evolution operator

$$\hat{U}(t, 0) = e^{-\frac{i}{\hbar}\hat{H}t} = e^{-i\omega t\hat{\sigma}_x} = \cos(\omega t)\hat{\mathbb{I}} - i\sin(\omega t)\hat{\sigma}_x. \quad (2)$$

Initializing the state of the qubit on  $|0\rangle$ , it evolves into an oscillation between the two logic states with frequency  $\omega$

$$|\psi(t)\rangle = \hat{U}(t, 0)|0\rangle = \cos(\omega t)|0\rangle - i\sin(\omega t)|1\rangle. \quad (3)$$

The probability for the qubit to be found on its initial state (survival probability) will be denoted by

$$p(t) = |\langle 0|\psi(t)\rangle|^2. \quad (4)$$

\* correspondence at: [simone.paganelli@univaq.it](mailto:simone.paganelli@univaq.it)

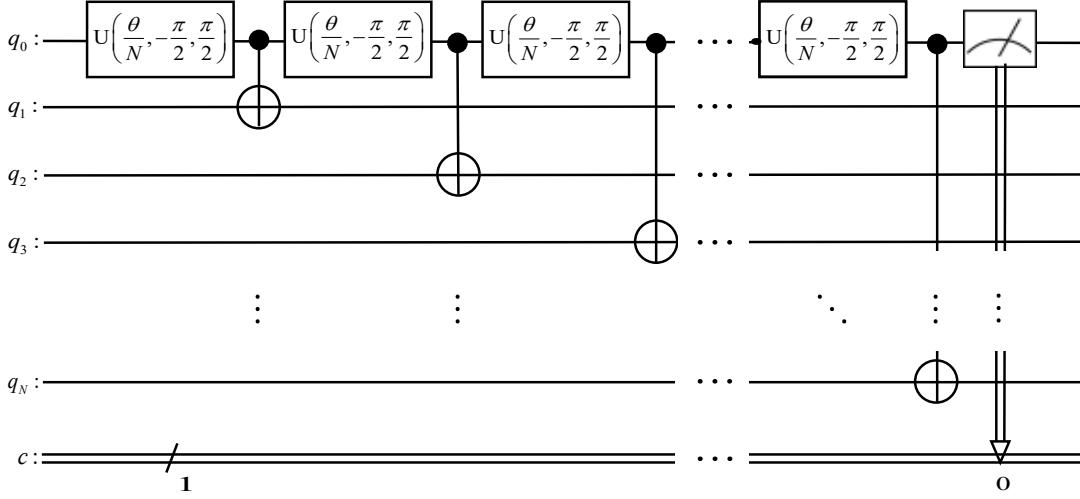


Figure 1. Schematic circuit employed in the qasm simulations. To simulate Rabi oscillations, we employ the rotation in Eq. (6) where  $\lambda = -\phi = \frac{\pi}{2}$  is fixed and  $\theta$  plays the role of the evolution time. For the  $N$  intermediate measurements during the evolution we need the same number of ancillary qubits. So the full rotation is divided into  $N$  equivalent rotations, each of one followed by a  $CNOT$  gate.

For  $t \ll \frac{1}{\omega}$ , if  $N$  projective measurements are performed at intervals  $\Delta t = \frac{t}{N}$ , the time evolution changes into

$$p_{QZE}(t) = \left[ p\left(\frac{t}{N}\right) \right]^N \simeq \left( 1 - \omega^2 \frac{t^2}{N^2} \right)^N \xrightarrow{N \gg 1} e^{-\frac{\omega^2 t^2}{N}}, \quad (5)$$

leading to the QZE. The oscillations driven by the Rabi evolution have been implemented using the single-qubit rotation gate

$$\hat{U}_{\theta, \phi, \lambda} = \begin{bmatrix} \cos \frac{\theta}{2} & -e^{i\lambda} \sin \frac{\theta}{2} \\ e^{i\phi} \sin \frac{\theta}{2} & e^{i(\phi+\lambda)} \cos \frac{\theta}{2} \end{bmatrix}, \quad (6)$$

and fixing  $\phi = -\frac{\pi}{2}$ ,  $\lambda = \frac{\pi}{2}$  and  $\theta = 2\omega t$ . To emulate the measurement we did not use the corresponding irreversible gate, but we employed  $CNOT$  gates and the entanglement among the states of different qubits. Given a normalized state for the system qubit  $|\psi\rangle = \alpha|0\rangle + \beta|1\rangle$ , its density matrix is

$$\hat{\rho}_{\text{in}} = |\psi\rangle\langle\psi| = \begin{bmatrix} |\alpha|^2 & \alpha\beta^* \\ \alpha^*\beta & |\beta|^2 \end{bmatrix}. \quad (7)$$

Introducing an ancillary target qubit in the state  $|0\rangle$ , the action of the  $CNOT$  gate on the two qubits is  $|\phi\rangle = CNOT(|\psi\rangle \otimes |0\rangle) = \alpha|00\rangle + \beta|11\rangle$  and evaluating the reduced density matrix related to the state of the system qubit, one gets

$$\hat{\rho}_{\text{fin}} = \begin{bmatrix} |\alpha|^2 & 0 \\ 0 & |\beta|^2 \end{bmatrix}, \quad (8)$$

which is exactly the density matrix that one would obtain after a projective measurement process. The ideal setup is depicted in Fig. 1, where each rotation produces the

intermediate Rabi evolution between every measurement, implemented by the  $CNOT$  gates.

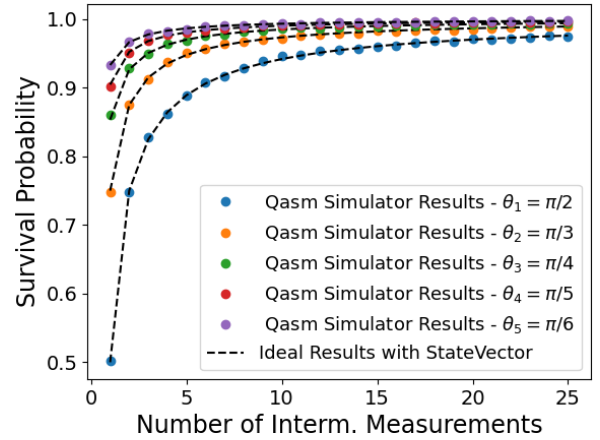


Figure 2. Survival probability of an ideal qubit in the initial state, i.e.  $|0\rangle$ , depending on the number of intermediate measurements applied during the evolution at fixed  $\theta$ .

In the ideal case, imposing that each  $CNOT$  has a negligible runtime, the total evolution time can be fixed as  $\theta = 2\omega t$ . In Fig. 2 we show the results of the simulations for different durations of the total evolution which are in agreement with the results shown in [31]. The ideal points are obtained through statevector simulations which produce for the final state the probability amplitudes of each element of the computational basis. To reproduce the real experiment, simulations were performed also using qasm simulator backend from Qiskit Aer, producing randomly distributed final measurement outputs. The weights of each component of the final state

are thus reconstructed from the statistics of the outputs of the same repeated experiments. In order to have an accurate statistical description, we ran each quantum circuit 20000 times. As expected, for each  $\theta$ , the survival probability in the initial state increases towards one as the number of intermediate measurements increases as well, freezing the Rabi oscillations.

In this ideal case, the Rabi dynamics is assumed to be dominant with respect to any other dissipative effect. A real qubit is affected by decoherence processes due to the interaction with the external environment. These are the so called relaxation and dephasing: the former is associated to the spontaneous decay process from the excited state to the ground one in a non-unitary way and it has a characteristic time  $T_1$ , while the latter is related to the phenomenon which leads from a pure state to a mixed one, by suppressing the non-diagonal elements of the density matrix, and it is characterized by a specific  $T_2$ . It is important to highlight that, for the qubits of the devices provided by the IBM Quantum Experience,  $T_1$  and  $T_2$  are generically of tens or hundreds  $\mu s$  in order of magnitude, and that the different gates are nothing but pulses with precise running times ( $\langle \Delta t_{\text{single-qubit gates}} \rangle \simeq 35.7 ns$  and  $\langle \Delta t_{CNOT} \rangle \simeq 300 ns$ ). Therefore, in the implementation on the real device, we expect that increasing the number of operations, the decoherence becomes relevant.

The second case that we considered is the natural decay of the qubit. In the NISQ devices, for each qubit only one of the two computational states is stable, say  $|0\rangle$ , so after initializing the qubit on  $|1\rangle$  we expect a relaxation to the ground state  $|0\rangle$  due to the noise. The survival probability in the initial state is

$$p(t) = \langle 1 | \hat{\rho}(t) | 1 \rangle. \quad (9)$$

Also in this case, after initializing the qubit in its excited state, we try to freeze the spontaneous decay towards  $|0\rangle$  introducing repeated measurements. As in the previous case, the measurements are implemented by ancillary qubits and  $CNOT$  gates. In order to observe the QZE, we must consider the two decoherence effects which become significant around  $T_1$  and  $T_2$ , imposing as a condition that the observation time  $t$  should be such that  $t \ll T_2 \ll T_1$  [34]. The estimation of the observation time was done as follows. After the choice of a specific qubit on a certain device, we fixed a number of intermediate measurements and the total time  $t$ , which is given by the running times of all the gates employed, the read-out time (all these data are accessible on IBM Quantum Experience) and some intermediate temporal delays.

### III. IMPLEMENTATIONS ON A REAL DEVICE

In this section we report the results of the experiments carried out on an IBM Quantum Experience real device. The implementation on a real quantum computer is naturally affected by the noise which is not negligible. The

application of gates produces errors related to the discretization of their continuous parameters, but it can also introduce additional noise, especially when more qubits are involved, since a multi-qubits gate causes an interaction among qubits which enhances the decoherence effects.

Moreover, the specific design of the quantum computer must be considered. Real devices are characterized by a specific coupling map which describes the physical connections between qubits. Since two-qubits gates can be directly applied only on connected qubits, the implementation on the real device must be adapted accordingly. In Fig. 3 is reported the coupling map of the devices `ibm_nairobi`, `ibm_perth` and `ibmq_lima`. The device `ibm_nairobi` is the one we have employed to simulate the Rabi dynamics of a qubit.

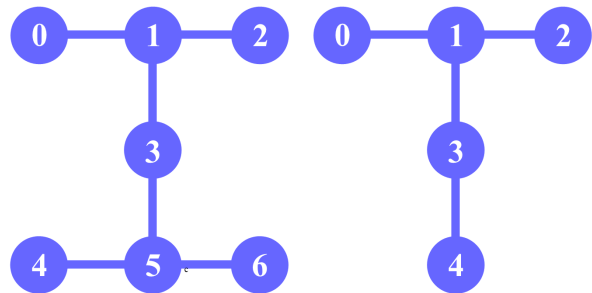


Figure 3. Coupling maps of the devices `ibm_nairobi` and `ibm_perth` (on the left) and `ibmq_lima` (on the right). Each number is associated to a certain qubit, and every map describes how the different systems interact among them.

We consider the evolution of the qubit number 5, being the most connected and therefore suitable to be coupled directly to qubits 3, 4 and 6 by  $CNOT$  gates. This allows us to reduce the time of execution, reducing the occurrence of the decoherence. To simulate the Rabi dynamics we prepared the circuit depicted in Fig. 4 with maximum level of optimization, reorganizing the order of the qubits accordingly to the coupling map. The survival probability has been measured for different numbers of intermediate measurements and the results, reported in Fig. 5, are qualitatively consistent with the ideal ones. There is also a quantitative good agreement, which is however limited from decoherence: in fact, in addition to statistical fluctuations, we can notice that the survival probability does not saturate to one but, with the increasing of the number of intermediate measurements, it tends to underestimate the expected values.

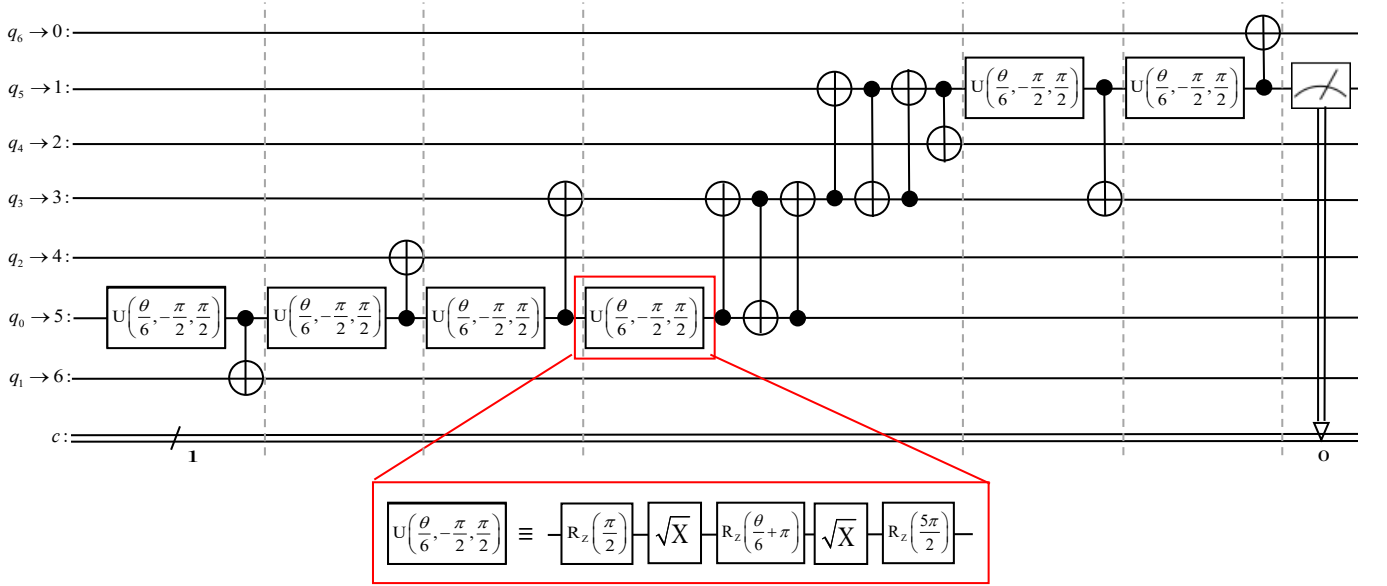


Figure 4. Circuit for the realization of the experiment with Rabi evolution on a real device, `ibm_nairobi`, starting from qubit 5. The implementation of the circuit is reorganized taking into account the constraints of the device, i.e. the coupling map showed in Fig. 3 and the gates which can be actually realized. In fact, every machine can perform only a reduced set of simple specific gates that can be used to construct all the others, as we can see with the  $U$  gate in the inset. To produce interaction between qubits which can not directly communicate, it is possible to apply three consecutive  $CNOT$  gates alternating target and control, to get a  $SWAP$  gate.

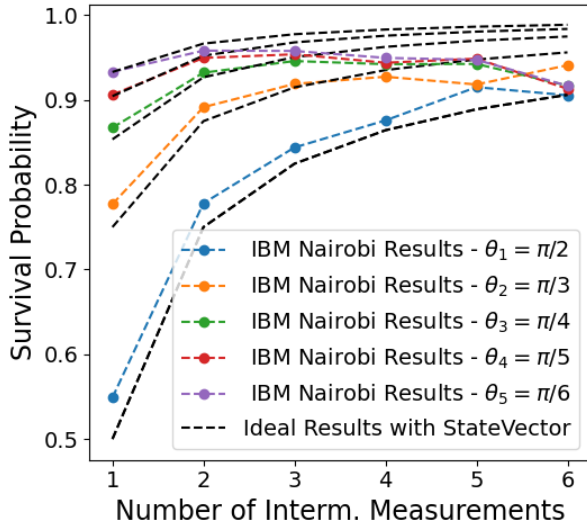


Figure 5. The survival probability in the  $|0\rangle$  state of the qubit number 5 belonging to the device `ibm_nairobi` as a function of the number of intermediate measurements introduced during the evolution at fixed  $\theta$  in comparison with the ideal results evaluated by `statevector.simulator`.

Due to the unavoidable coupling of the system with the environment, the evolution of the qubit is affected by relaxation and dephasing. As a consequence, we expect to observe on the real device the QZE also without imposing any dynamics, such as the Rabi one, but simply initializing the qubit's state in the excited one and leaving it free

to evolve. We stated in Section II that the condition to have a quadratic behavior of the survival probability is  $t \ll T_2 \ll T_1$ , where  $t$  is the observation time and  $T_1$ ,  $T_2$  are the decoherence times respectively for the relaxation and the dephasing. Taking into account that  $T_1$  and  $T_2$  could change daily, or even hourly, we performed at different times and days the experiment for all the qubits of all the machines available on the IBM Quantum Experience platform until the 10<sup>th</sup> of September 2023. An example of the implemented quantum circuits with the employment of delays for the observation of the QZE with the state of a qubit which freely evolves is shown in Fig. 6 and refers to the device `ibm_nairobi`.

In Tab. I are reported the data related to the clearest outputs obtained from the devices `ibm_nairobi`, `ibmq_lima` and `ibmq_perth`, and they are plotted in Figs. 7, 8, 9 in comparison with the decay function

$$p(t) = \left(1 - \frac{t^2}{N^2 T^2}\right)^N, \quad (10)$$

where  $T$  is the corresponding Zeno time.

The Eq. (10) can be easily obtained following the same steps showed in Eq. (5) considering a generic time-independent Hamiltonian  $\hat{H}$  and defining

$$T^2 = \frac{\hbar^2}{\langle \psi, 0 | \hat{H}^2 | \psi, 0 \rangle - \langle \psi, 0 | \hat{H} | \psi, 0 \rangle^2}. \quad (11)$$

The experimental data qualitatively follow the behavior

Device	Qubit	Date and Time	Obs Time [ $\mu s$ ]	$T$ [ $\mu s$ ]
ibm_perth	qr <sup>[0]</sup>	May 15, 2023 2:08 AM	$2.667 \pm 0.011$	$5.61 \pm 0.06$
ibm_nairobi	qr <sup>[2]</sup>	May 13, 2023 1:07 PM	$10.25 \pm 0.02$	$15.8 \pm 1.1$
ibm_nairobi	qr <sup>[2]</sup>	May 15, 2023 2:26 AM	$10.25 \pm 0.02$	$15.8 \pm 0.5$
ibmq_lima	qr <sup>[4]</sup>	May 13, 2023 2:06 AM	$10.48 \pm 0.02$	$16.0 \pm 0.4$
ibmq_lima	qr <sup>[4]</sup>	Sep 10, 2023 11:39 PM	$10.48 \pm 0.02$	$17.5 \pm 0.5$
ibmq_lima	qr <sup>[4]</sup>	Sep 10, 2023 5:10 PM	$8.380 \pm 0.014$	$14.5 \pm 0.4$

Table I. Evaluation of the Zeno time  $T$  for different devices and qubits. In the last column we show the value of the Zeno time obtained by comparing the experimental data with the theoretical function  $p(t) = \left[1 - \left(\frac{t}{NT}\right)^2\right]^N$ , where  $N$  is the fixed maximum number of implicit measurements and  $t$  is the evolution time.

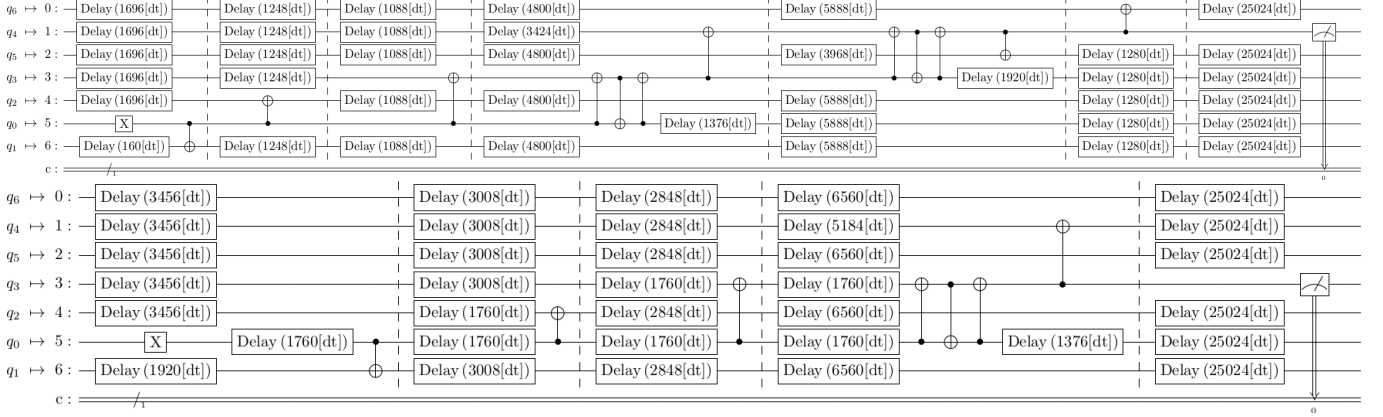


Figure 6. Circuits for the observation of the QZE during the spontaneous decay from  $|1\rangle$  to  $|0\rangle$  of the state of qubit number 5 of **ibm\_nairobi** with respectively six and four intermediate measurements. The former's running time is  $41024dt$ , while the latter is characterized by  $40896dt$  ( $1dt = 0.2ns$  in double precision). Three successive *CNOT* gates disposed as shown in here realizes a *SWAP* gate, whose effect is to exchange the states of the qubits involved. This is a necessary step when we want to entangle the states of two qubits that can not directly interact due to the coupling map of the device.

of Eq. (10) with some  $T$ . In Fig. 7 we observe a worse agreement with Eq. (10). A possible explanation is that the more the multiple measurements are, the longer is the total time of observation, and this enhances the decoherence effects. The fluctuations among the different outputs related to the same device and to the same qubit are due to frequent processes of recalibration of the decoherence times of the different systems.

Furthermore, we have to consider that, according also to Fig. 6, the measurements are not accurately equally-spaced in time, given the introduction in some cases of the *SWAP* gate formalized through three adjacent *CNOT* gates which are appropriately disposed. Nevertheless, what matters most in order to observe the QZE is to remain inside the temporal constraints imposed by the decoherence times, but this issue does not allow us to realize a proper fit with the function in Eq. (10) which was found instead for equally-spaced measurements.

Another detrimental element, always related to the *SWAP* gate, is the fact that we can not make interact directly the totality of the qubits of a certain device. This implies the need for such a gate, which exchanges the states of two adjacent qubits, with a further enhancement of decoherence.

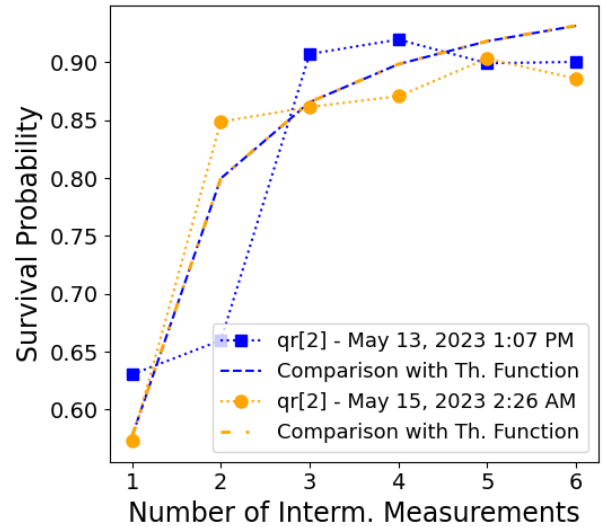


Figure 7. The evolution of the state of qubit number 2 of the device **ibm\_nairobi** fixing the maximum number  $N$  of intermediate measurements at  $N = 6$ . The blue dashed line corresponds to  $T = (15.8 \pm 1.1)\mu s$ , while the orange one to  $T = (15.8 \pm 0.5)\mu s$ .

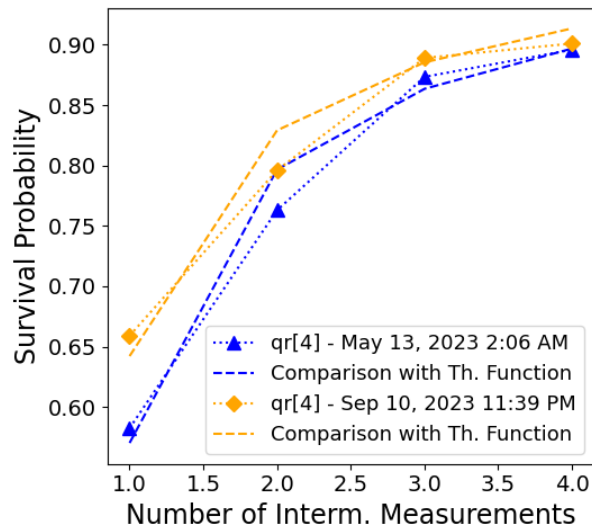


Figure 8. The evolution of the state of qubit number 4 of the device `ibmq_lima` fixing the maximum number  $N$  of intermediate measurements at  $N = 4$ . The blue dashed line corresponds to  $T = (16.0 \pm 0.4)\mu s$ , while the orange one to  $T = (17.5 \pm 0.5)\mu s$ .

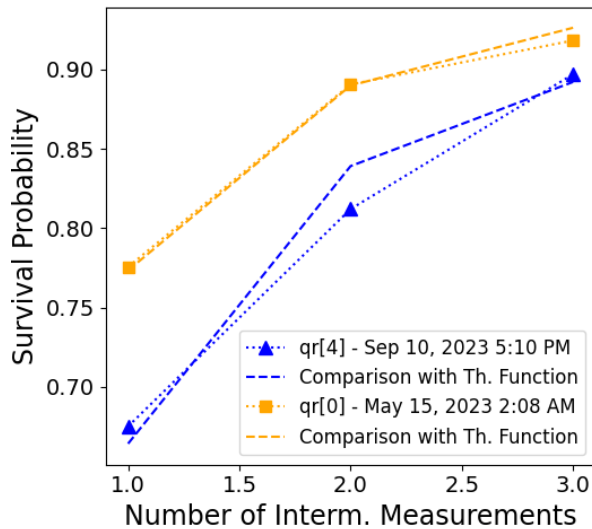


Figure 9. Evolution of the state of qubit number 4 of the device `ibmq_lima` (blue lines), compared with the theory with  $T = (14.5 \pm 0.4)\mu s$  (dashed line). Evolution of the state of qubit number 0 of the device `ibmq_perth` (orange lines), compared with the theory with  $T = (5.61 \pm 0.06)\mu s$  (dashed line). In both cases, the maximum number  $N$  of intermediate measurements is fixed at  $N = 3$ .

We notice that there is also an uncertainty on the evolution time  $t$ , as we can observe in Fig. 6. As we already said, we introduced some delays in order to compare experiments at fixed  $t$ . The evaluation of a delay depends on the temporal constraints imposed by the device we are working with. In fact, a physical device supports temporal intervals which are multiple of  $dt$ . In partic-

ular,  $1dt = 0.2$  (in double precision) and it represents a discretization unit of temporal pulses sent as input to the machine. The granularity for the duration of a delay, that is the unit of time of which a delay should be multiple, is the least common multiple between the `pulse_alignment` and the `acquire_alignment`. In each analyzed case, we had `granularity = 16dt`. As a consequence, the delay communicated to the device is an integer multiple of such a value, corresponding to an approximation by excess or by defect of the time we really want to wait before the application of a certain gate. In the worst case, all the delays are approximated by excess (defect) and this leads to an error on the total evolution time which is equal to  $N(16dt)$ , where  $N$  is the number of the total necessary delays, which coincides at most with the fixed maximum number of intermediate measurements.

All these issues lead to an estimation of different values of the Zeno time (but they all are of the order of  $10\mu s$ ) and to a general tendency of the experimental data to underestimate the comparison function with the increase of the intermediate measurements. Despite that, the results of the experiments showed a QZE on trasmon qubits which freely evolve starting from the unstable state  $|1\rangle$ .

#### IV. CONCLUSIONS

In this paper we reported the observation of the QZE on IBM NISQ devices. We studied for a single qubit its survival probability on the initial state after the effect of multiple measurements.

We first employed the quantum circuit to mimic a Rabi time-evolution, as first proposed by [31], introducing a set of *CNOT* gates to perform the intermediate measurements. After a first simulation by Qasm we reproduced the experiment on a real device finding a net reduction of the oscillating rate, with a good qualitative agreement with the simulation.

We also tried to observe the QZE during the free evolution of the state of a qubit from the unstable one  $|1\rangle$  to  $|0\rangle$ . While in the previous case to observe the QZE the time distance between two subsequent measurements had to be much smaller than the Rabi period, here it has to be much smaller than the decoherence times. Unfortunately, we do not have a full control of the decoherence times, since they are continuously recalibrated, and additionally each circuit is inserted in a queue that could be roughly long during which  $T_1$  and  $T_2$  may change. This is why in this case the observation of the QZE turned out to be more demanding. Some qubits exhibit decoherence times with very little relative variations: there are some qubits which more easily show the QZE, but for a more quantitative analysis of the reason why some qubits show this behavior rather than others it could be important to have precise information about the Hamiltonian of the single qubit under examination. The platform IBM Quantum Experience allows us to know formally the Hamiltonian

of each device, but we could not be able to have access to more specific information about the parameters of those Hamiltonians.

As it is shown in Section III, we were able to observe the Quantum Zeno Effect in both simulations and experiments.

**Acknowledgements** – The authors acknowledge IBM. IBM, the IBM logo and ibm.com are trademarks of International Business Machines Corp., registered

in many jurisdictions worldwide. Other product and service names might be trademarks of IBM or other companies. The current list of IBM trademarks is available (see <https://www.ibm.com/legal/copytrade>). S. P. and C. C. acknowledge financial support from the University of L'Aquila by the internal project "Variational Quantum Eigensolver methods for the disordered Su-Schrieffer-Heeger model"

- 
- [1] A. Degasperis, L. Fonda and G. C. Ghirardi, *Does the lifetime of an unstable system depend on the measuring apparatus?*, *Il Nuovo Cimento A* **21**, 471 (1974).
- [2] B. Misra and E. C. G. Sudarshan, *The Zeno's paradox in quantum theory*, *Journal of Mathematical Physics* **18**(4), 756–763 (1977).
- [3] C. B. Chiu, E. C. G. Sudarshan and B. Misra, *The time evolution of unstable quantum states and a resolution of Zeno's paradox*, *Phys. Rev. D* **16**(2), 520- (1977).
- [4] E. Joos, *Continuous measurement: Watchdog effect versus golden rule*, *Phys. Rev. D* **29**, 1626 (1974).
- [5] Richard J. Cook, *What are Quantum Jumps?*, *Physica Scripta* **1988**(T21) (1988).
- [6] H. Nakazato, M. Namiki, S. Pascazio and H. Rauch, *Understanding the quantum Zeno effect*, *Phys. Lett. A* **217**(4), 203–208 (1996).
- [7] C. Presilla, R. Onofrio and U. Tambini *Measurement Quantum Mechanics and Experiments on Quantum Zeno Effect* *Annals of Physics* **248**, 95121 (1996)
- [8] P. Facchi, G. Marmo and S. Pascazio, *Quantum Zeno dynamics and quantum Zeno subspaces*, *J. Phys.: Conf. Ser.* **196**(1), 012017 (2009).
- [9] S. Pascazio, *All You Ever Wanted to Know About the Quantum Zeno Effect in 70 Minutes*, *Open Sys. Inf. Dyn.* **21**(01n02), 1440007 (2014).
- [10] F. Giacosa, *Non-exponential Decay in Quantum Field Theory and in Quantum Mechanics: The Case of Two (or More) Decay Channels*, *Foundations of Physics* **42**(10), 1262–1299 (2012).
- [11] U. Lucia, *Irreversible and quantum thermodynamic considerations on the quantum zeno effect*, *Scientific Reports* **13**(1), 10763 (2023).
- [12] Wayne M. Itano, D. J. Heinzen, J. J. Bollinger and D. J. Wineland, *Quantum Zeno effect*, *Phys. Rev. A* **41**(5), 2295–2300 (1990).
- [13] P. Kwiat, H. Weinfurter, T. Herzog, A. Zeilinger, M. A. Kasevich, *Interaction-Free Measurement*, *Phys. Rev. Lett.* **74**(24), American Physical Society, 4763–4766 (1995).
- [14] B. Nagels, L. J. F. Hermans, P. L. Chapovsky, *Quantum Zeno Effect Induced by Collisions*, *Phys. Rev. Lett.* **79**(17), American Physical Society, 3097–3100 (1997).
- [15] K. Mølhave and M. Drewsen, *Demonstration of the continuous quantum Zeno effect in optical pumping*, *Physics Letters A* **268**(1), 45–49 (2000).
- [16] M. C. Fischer, B. Gutiérrez-Medina, M. G. Raizen, *Observation of the Quantum Zeno and Anti-Zeno Effects in an Unstable System*, *Phys. Rev. Lett.* **87**, 040402 (2001).
- [17] B. Zhu, B. Gadway, M. Foss-Feig, J. Schachenmayer, M. L. Wall, K. R. A. Hazzard, B. Yan, S. A. Moses, J. P. Covey, D. S. Jin, J. Ye, M. Holland, A. M. Rey, *Suppressing the Loss of Ultracold Molecules Via the Continuous Quantum Zeno Effect*, *Phys. Rev. Lett.* **112**, 070404 (2014).
- [18] P. Facchi, S. Pascazio, *Quantum Zeno Subspaces*, *Phys. Rev. Lett.* **89**, 080401 (2002).
- [19] P. Facchi, D. A. Lidar, S. Pascazio, *Unification of dynamical decoupling and the quantum Zeno effect*, *Phys. Rev. A* **69**, 032314 (2004).
- [20] P. Facchi, R. Fazio, G. Florio, S. Pascazio, T. Yoneda, *Zeno Subspaces for Coupled Superconducting Qubits*, *Foundations of Physics* **36**, 500 (2006).
- [21] P. Facchi, M. Ligabò, *Quantum Zeno effect and dynamics*, *Journal of Mathematical Physics* **51**, 022103 (2010).
- [22] S. Hacoheh-Gourgy, L. P. García-Pintos, L. S. Martin, J. Dressel, I. Siddiqi, *Incoherent Qubit Control Using the Quantum Zeno Effect*, *Phys. Rev. Lett.* **120**(2), American Physical Society, 020505 (2018).
- [23] P. Facchi, S. Tasaki, S. Pascazio, H. Nakazato, A. Tokuse, D. A. Lidar, *Control of decoherence: Analysis and comparison of three different strategies*, *Phys. Rev. A* **71**(2), American Physical Society, 022302 (2005).
- [24] L. Fonda, G. C. Ghirardi and A. Rimini, *Decay theory of unstable quantum systems*, *Reports on Progress in Physics*, **41**(4), 587 (1978).
- [25] H. Nakazato, M. Namiki, S. Pascazio, *Temporal behavior of quantum mechanical systems*, *International Journal of Modern Physics B*, **10**(03), 247 (1996).
- [26] A. G. Kofman and G. Kurizki, *Frequent Observations Accelerate Decay: The anti-Zeno Effect*, *Zeitschrift für Naturforschung A* **56**(1-2), 83–90 (2001).
- [27] P. Facchi, H. Nakazato, S. Pascazio, *From the Quantum Zeno to the Inverse Quantum Zeno Effect*, *Phys. Rev. Lett.* **86**(13), American Physical Society, 2699–2703 (2001).
- [28] I. Antoniou, E. Karpov, G. Pronko, E. Yarevsky, *Quantum Zeno and anti-Zeno effects in the Friedrichs model*, *Phys. Rev. A* **63**(6), American Physical Society, 062110 (2001).
- [29] K. Na, *Revisiting quantum Zeno effect and anti-Zeno effect: Universality vs non-universality*, *Journal of Mathematical Physics* **62**(12), 122101 (2021).
- [30] M. Lewenstein, K. Rzażewski, *Quantum anti-Zeno effect*, *Phys. Rev. A* **61**(2), 022105 (2000).
- [31] S. Barik, D. K. Kalita, B. K. Behera, P. K. Panigrahi, *Demonstrating quantum zeno effect on IBM Quantum Experience*, arXiv preprint arXiv:2008.01070 (2020).
- [32] J. Sudhanva, *Realization of Quantum Zeno Ef-*

- fect on IBM Quantum Experience and QISKIT, DOI:10.13140/RG.2.2.26141.18409.
- [33] D. Šafránek, S. Deffner, *Quantum Zeno effect in correlated qubits*, *Phys. Rev. A* **98**, 032308 (2018).
- [34] Y. Matsuzaki, S. Saito, K. Kakuyanagi, and K. Semba, *Quantum Zeno effect with a superconducting qubit*, *Physical Review B* **82**, 180518 (2010).
- [35] K. Kakuyanagi, T. Baba, Y. Matsuzaki, H. Nakano, S. Saito and K. Semba, *Observation of quantum Zeno effect in a superconducting flux qubit*, *New J. Phys.* **17**, 063035 (2015).
- [36] P. M. Harrington, J. T. Monroe and K. W. Murch, *Quantum Zeno Effects from Measurement Controlled Qubit-Bath Interactions*, *Phys. Rev. Lett.* **118**, 240401 (2017).
- [37] K. Bharti et al. *Noisy intermediate-scale quantum algorithms*, *Rev. Mod. Phys.* **94**, 015004 (2022).
- [38] M. H. Devoret, A. Wallraff, J. M. Martinis, *Superconducting qubits: A short review*, *arXiv preprint cond-mat/0411174* (2004).
- [39] A. F. Kockum, F. Nori, *Quantum Bits with Josephson Junctions*, Springer International Publishing, 703–741 (2019).
- [40] J. Koch, T. M. Yu, J. Gambetta, A. A. Houck, D. I. Schuster, J. Majer, A. Blais, M. H. Devoret, S. M. Girvin, R. J. Schoelkopf, *Charge-insensitive qubit design derived from the Cooper pair box*, *Phys. Rev. A* **76**(4), 042319 (2007).